1999 Conference on Control Applications
22-27 August 1999

A Testbed for Nonlinear Flight Control Techniques: The Caltech Ducted Fan [1]

Mark Milam
milam@cds.caltech.edu

Richard M. Murray
murray@indra.caltech.edu

Division of Engineering and Applied Science
California Institute of Technology
Pasadena, California 91125

Abstract

This paper considers the fundamental design and modeling of the Caltech ducted fan. The Caltech ducted fan is a scaled model of the longitudinal axis of a flight vehicle. The purpose of the ducted fan is the research and development of new nonlinear flight guidance and control techniques for Uninhabited Combat Aerial Vehicles. It is shown that critical design relations must be satisfied in order that the ducted fan's longitudinal dynamics behave similar to those of an flight vehicle. Preliminary flight test results illustrate the flying qualities of the ducted fan.

Keywords: Flight Control Experiment, Uninhabited Combat Air Vehicle, Flight Vehicle Simulator

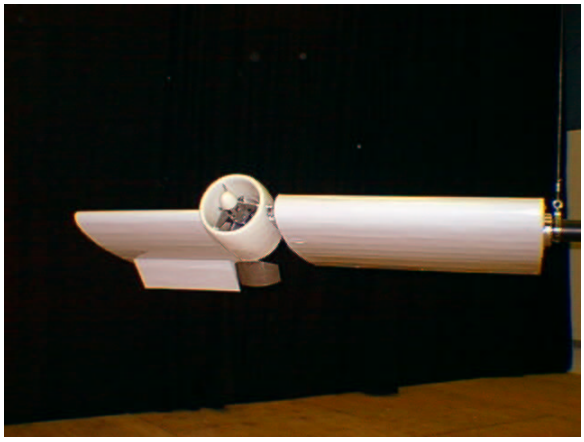

Figure 1: Caltech Ducted fan

1 Introduction

Uninhabited combat air vehicles (UCAVs) are moving closer to reality. Recently, several military contractors have revealed plans for the next-generation, pilot less fighters [2], [9]. The operator of such a fighter would be located far away in a ground or airborne based control room containing virtual-reality technology allowing the operators to direct the UCAVs easily. The idea of directly commanding the actuators, as in a typical aircraft, would be impractical considering the workload, redundant actuators, and fast dynamics of a typical UCAV. Instead, either the desired objective would be commanded by the operator or pre-programmed without operator intervention. The UCAV would autonomously determine the control actuation to follow the desired objective while simultaneously satisfying the system equations. The desired objective may be to go to a single point, or pass through several waypoints, or track a target. The main advantage of not having a pilot on board is that the planes performance does not need to be stifled to ensure pilot survivability. As a result, the UCAV will autonomously fly highly aggressive trajectories, frequently on the fringe of the flight envelope, testing all conventional flight control theory to date.

At Caltech, we have built a scaled model of the longitudinal axis of a flight vehicle in order to develop the new guidance, surface allocation, and flight control theory and algorithms needed for these advanced UCAV's. The successful development of two other control experiments outlined in [5] and [7] prove that such a task is realistic. Requirements for our testbed were twofold: First, conclusions and future directions concerning the guidance and control UCAV's could be identified, and second, risks of catastrophic failure and costs of the testbed had to be minimized.

The Caltech ducted fan is an indoor flying, tethered representation of the longitudinal dynamics of a flight vehicle. A picture of the ducted fan is shown in Figure 1. Thrust vectoring gives the ducted fan a large flight envelope while easy reconfigurability provides the ducted fan with a variety of stability and modeling options.

[1] Research funded in part by AFOSR grant F49620-95-1-0419

In order to realistically emulate the longitudinal dynamics of a flight vehicle, a number of design considerations were taken into account. The dynamics of tethering, constrain the operation of the ducted fan on a large cylinder, were designed in such a way that the overall system dynamics behaved like that of a flight vehicle from the ducted fan's point of view.

The organization of this paper is as follows: First, a detailed description of the hardware design is discussed. Second, a first principles model will be deduced illustrating critical design variables. Third, results of preliminary open loop flight tests are presented. Finally, the last section summarizes our main conclusions and indicates future work.

2 Experimental Setup

The primary components of the Caltech ducted fan experiment are shown in Figure 2.

The aluminum stand and boom limit the operation of the ducted fan to a cylinder of radius 2.35 m and height of 4 m. Revolute joints at the base and end of the boom provide two rotational degrees of freedom while a prismatic joint parallel to the stand provides a translational degree of freedom.

The primary design consideration for all three joints was to minimize friction in the presence of the cantilevered ducted fan (5 kg at 2.5 m). Both the revolute joint at the base and the revolute joint at the end of the boom use two low-friction radial ball bearings. The bearings are mounted in-line an appropriate distance apart, parallel to their respective axes of rotation, to mitigate the moment loads. Motion along the prismatic joint is provided by two parallel stainless steel rails. Several different off-the-shelf linear bearings, including recirculating ball bearing and needle bearing pillow blocks, were tested on the rails. None of these bearings provided the sufficient low friction under the large moment loads. After many design iterations, four custom built radial ball bearing pillow blocks provided the necessary friction characteristics. Each bearing pillow blocks contained triad of low friction angular contact radial ball bearings . The pillow blocks were mounted on the rails 0.5 m apart, two for each rail.

In order to prevent the boom and ducted fan from a catastrophic failure along the vertical direction, the stand is equipped with three mechanical brakes. The operation of the brakes are similar in design to the the cable harness on an aircraft carrier. In our case the mechanical brakes convert the kinetic energy of boom and ducted fan into potential energy by means of three torsional springs. A spring loaded ratchet and pawl

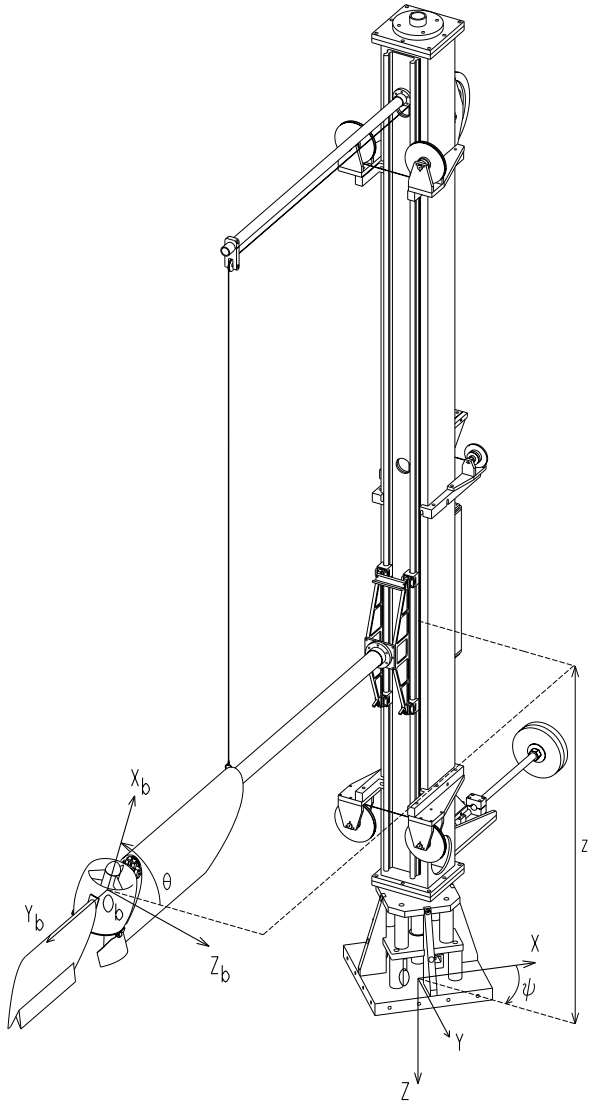

Figure 2: The Caltech Ducted Fan Testbed

prevent the torsional springs from unloading.

Signals are routed through the stand and boom through two slip rings. Each slip ring has 26 channels rated at 2 amps per channel. The slip rings are mounted at the two revolute joints. Three optical encoders with resolution of 0.18 degrees are used to sense the motion of the system. Optical encoders are mounted at the revolute joints and on the counterbalance pulley mechanism.

A counterbalance system was required since the maximum thrust of the ducted fan engine is limited to 18 N while the weight of the boom and fan is 10 kg. The counterweight rides on two linear recirculating ball bearing pillow blocks. The "effective" gravity of the system was initially set to 0.075 g by adding lead shot to the counterweight. The unique feature of the counterbalance is the a pulley system that provides a 4 to 1 gear ratio. That is, for every 1 m the boom and ducted

fan move the counterweight moves 0.25 m. Gearing the system in this way allows us an increase in the maximum vertical acceleration of the ducted fan.

The ducted fan's primary components are the wings and engine. In order that the system by able to fly in both directions, the wings and engine were designed to be symmetric. The engine shroud was constructed using urethane foam with an aluminum frame. The shroud houses a 0.1524 m diameter Byron ducted fan propeller. The power plant is an Astroflight Cobalt 40 electric motor. An Advanced Motions power amplifier, which regulates the commanded current, provides the power to the motor. Thrust vectoring of the ducted fan is provided by two aluminum paddles driven by pwm servos. The wings primary construction material is balsa wood. The wings center of pressure is adjustable within approximately +/- 0.06 m of the center of mass of the system. The center of mass of the fan and engine may be aligned up with the axis of rotation by means of a screw driven x-y positioner. A NACA 0026 wing section [3] was chosen as the inboard wing while a NACA 0015 was chosen as the outboard wing. A thicker wing section was chosen for the inboard wing since it was required to rotate about the 0.0635 m diameter boom. Both wing chords were chosen to be 0.5080 m. The inboard wing also has a custom ball bearing at the tip rotating on the boom to add additional stiffness to the system. The outboard wing has an elevator with a chord of 0.14 m. The elevator, like the paddles, is actuated by a pwm servo.

All guidance control laws and signal conditioning are hosted on a dSPACE system [1]. The Texas Instrument TMS320C40 60MHz and Digital Equipment Corporation 21164 500 MHz signal processors provide computational power for our testbed. An incremental encoder,multi-purpose digital I/O, and the D/A dSPACE interface boards provide the interface to the pwm actuators, sensor optical encoders and joystick optical encoders, and power amplifier, respectively. The dSPACE software COCKPIT and two joysticks provide the operator with a variety of user interface options to the ducted fan testbed.

3 Equations of motion

In this section critical design relations are shown, by means of deriving the equations of motion that must be satisfied in order that the ducted fan's dynamics behave similar to the longitudinal dynamics of a flight vehicle. Figure 2 depicts the model as well as the coordinate systems of the ducted fan testbed that will be used throughout this section. The axis system located at the center of the ducted fan and rotating with it will be referred to as the body frame. Another axis system, the spatial frame, is located at the base of the stand and fixed to the experiment.

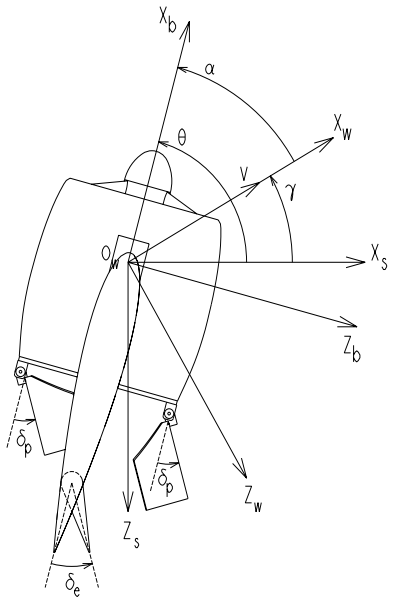

Figure 3: Ducted Fan Shroud and Wing Conventions

The following criterion, describing the general assumptions for longitudinal flight of an aircraft, will be used as the design goals for the ducted fan testbed.

1. Aircraft are symmetrical with respect to a vertical plane aligned through the longitudinal axis of the aircraft. For our system O_bX_b and O_bZ_b will lie in this plane of symmetry.

2. The motion of the aircraft behaves like that of a single rigid body on $SE(2)$ with applied forces and moments.

Both of these criterion place restrictions on the mass matrix of our system. A complete description of the qualitative behavior of an aircraft may be found in [4] and [6].

The configuration chosen for this system will be position of the stand along a cylinder centered at the origin of the spatial reference frame of length r_s, that is $x = \psi r_s$, the vertical position z of the ducted fan, and the the pitch angle of the ducted fan θ. We write $q = (x, z, \theta)$.

The inputs will be taken as the forces and moments $f_x^b, f_z^b, \tau_\theta^b$ due to thrust vectoring as well as the forces and moments $f_x^w, f_z^w, \tau_\theta^w$ due to aerodynamics. The thrust vectoring and aerodynamics are considered to be applied in the body and wind coordinate frames, respectively. The wind coordinate system, whose origin coincides with the body frame, is shown in Figure 3.

The angle of attack α and the flight path angle γ used to describe the wind coordinate frame may be described in terms of the configuration variables

$$\gamma = \arctan\frac{-\dot{z}}{-\dot{x}} \qquad \alpha = \theta - \gamma.$$

Applying Lagrange's equation [8], we would expect the form of the equations of motion to be the following:

$$M(q)\ddot{q} + C(q,\dot{q})\dot{q} + N(q) = \Upsilon.$$

$M(q)$ is the generalized mass matrix, $C(q,\dot{q})\dot{q}$ is the Coriolis matrix, $N(q)$ is the vector of gravity terms and Υ is the vector of generalized forces.

Satisfaction of our design goals is completely determined by the kinetic energy of our system since it alone determines the mass matrix in our case. For a single rigid body on $SE(2)$, we would expect that the mass matrix would be of the form

$$\begin{bmatrix} mI & 0 \\ 0 & J \end{bmatrix} \tag{1}$$

where m and J are the mass and inertia of the rigid body, respectively.

The kinetic energy for the ducted fan testbed is

$$\begin{aligned} K(q,\dot{q}) &= \frac{1}{2}I_Z(\frac{\dot{x}}{r_s})^2 + \frac{1}{2}I_{Y_b}\dot{\theta}^2 + \frac{1}{2}m_f\dot{z}^2 + \frac{1}{2}m_c\frac{\dot{z}^2}{r_g^2} \\ &\quad + \frac{1}{2}I_{X_b}(\frac{\dot{x}}{r_s})^2 s_\theta^2 + \frac{1}{2}I_{Z_b}(\frac{\dot{x}}{r_s})^2 c_\theta^2 \\ &\quad + \frac{1}{2}I_p(\Omega - \frac{\dot{x}}{r_s}s_\theta)^2. \end{aligned}$$

where I_z is the moment of inertia of the stand, counterweight, and fan about OZ, m_f, m_b, and m_c are the masses of the fan, boom, and counterweight, respectively. I_{X_b}, I_{Y_b}, and I_{Z_b} are moments of inertia of the ducted fan in body coordinates, I_p is the moment of inertia of the propeller and the electric motor, r_g is the gear ratio of the pulley, and Ω is the angular velocity of the propeller. In addition, we use the shorthand notation $c_\theta = \cos\theta$ and $s_\theta = \sin\theta$. In this paper the angular velocity of motor will be considered as a constant during any particular dynamic analysis. However, in general Ω is a function of the input current to the motor.

This kinetic energy alone determines the mass matrix for our system

$$M(q) = \begin{bmatrix} m_1(\theta) & 0 & 0 \\ 0 & m_2 & 0 \\ 0 & 0 & I_{Y_b} \end{bmatrix} \tag{2}$$

where

$$\begin{aligned} m_1(\theta) &= (I_Z + (I_{X_b} + I_p)c_\theta^2 + I_{Z_b}s_\theta^2)/r_s^2, \quad \text{and} \\ m_2 &= m_b + m_f + \frac{m_c}{r_g^2}. \end{aligned}$$

In order to make the mass matrix (2) the same along the x and z directions as in (1) the ducted fan testbed was designed such that $m_1(\theta) < m_2$. Once the system was assembled the mass properties were measured, more mass was affixed to the stand in order to make $m_1(\theta) = m_2$. The m_1 dependence on θ is very small and can be neglected since I_z is nearly 600 times larger than either I_{X_b}, I_{Z_b}, or I_p. In fact, the magnitude of I_{X_b}, I_{Z_b}, or I_p is within the uncertainty of measuring I_Z. In addition, assuming we can measure all the moments of inertia without uncertainty, $I_{X_b} + I_p$ is approximately equal to I_{Z_b} so that $m_1 = (I_z + I_{Z_b})/r_s$. There are no off-axis inertia terms since the ducted fan is completely symmetric about the O_bX_b and O_bY_b plane. Furthermore, the axis of rotation of the ducted fan is about its center of mass.

The Coriolis matrix for our system is

$$C(q,\dot{q}) = \begin{bmatrix} I_2\dot{\theta}s_\theta c_\theta & 0 & I_2\frac{\dot{x}}{r_s}s_\theta c_\theta - I_p\Omega c_\theta \\ 0 & 0 & 0 \\ I_p\Omega c_\theta - I_2\frac{\dot{x}}{r_s}s_\theta c_\theta & 0 & 0 \end{bmatrix}$$

where

$$I_2 = I_{X_b} + I_p - I_{Z_b}.$$

The $I_p\Omega c_\theta$ term can be considerably large when the propeller is rotating at 15000 r.p.m., thus it cannot be neglected. There is a noticeable positive pitching moment on the ducted fan when it is flying counterclockwise and a negative pitching moment when the ducted fan is flying clockwise for large $\dot{x}$. This effect is considered as a disturbance into the system since it is not characteristic of longitudinal flight. Since I_{Z_b} and $I_{X_b} + I_p$ are approximately equal and $\frac{\dot{x}}{r_s}$ and $\dot{\theta}$ are small in comparison to Ω, the terms containing the coefficient I_2 have negligible influence on the system dynamics.

From the potential energy of the system

$$V(q,\dot{q}) = m_2 z g$$

where

$$m_2 = \frac{m_c}{r_g} - m_b - m_f$$

we obtain the gravity vector

$$N(q,\dot{q}) = \begin{bmatrix} 0 \\ g(\frac{m_c}{r_g} - m_b - m_f) \\ 0 \end{bmatrix}.$$

The generalized forces Υ are given by

$$\Upsilon = \begin{bmatrix} -f_x^b c_\theta + f_z^b s_\theta - f_x^w \frac{r_a}{r_s}c_\gamma + f_z^w \frac{r_a}{r_s}s_\gamma \\ f_x^b s_\theta + f_z^b c_\theta + f_x^w s_\gamma + f_z^w c_\gamma \\ \tau_\theta^b + \tau_\theta^w \end{bmatrix} \tag{3}$$

where r_a is the radial distance from the center of the stand to the effective application point of the aerodynamic forces.

The ratio $\frac{r_a}{r_s}$ that appears in equation (3) is a result of the resultant aerodynamic force not being applied at a point on the symmetry plane. Due to the rotation of the ducted fan on the boom, the wings will experience increasing linear velocities as we move towards the tip of the outboard wing. Keeping in-line with our design goals, we will next illustrate how the wings were designed in order to make $r_a = r_s$.

The aerodynamic forces may be written

$$\begin{aligned} f_z^w &= -\frac{1}{2}C_{Li}\bar{c}_i\rho(\dot{\psi}^2\int_{r_{t_i}}^{r_{b_i}} r^2dr - \dot{z}^2\int_{r_{t_i}}^{r_{b_i}} dr) \\ &\quad -\frac{1}{2}C_{Lo}\bar{c}_o\rho(\dot{\psi}^2\int_{r_{b_o}}^{r_{t_o}} r^2dr - \dot{z}^2\int_{r_{b_o}}^{r_{t_o}} dr) \end{aligned}$$

and

$$\begin{aligned} f_x^w &= -\frac{1}{2}C_{Di}\bar{c}_i\rho(\dot{\psi}^2\int_{r_{t_i}}^{r_{b_i}} r^2dr - \dot{z}^2\int_{r_{t_i}}^{r_{b_i}} dr) \\ &\quad -\frac{1}{2}C_{Do}\bar{c}_o\rho(\dot{\psi}^2\int_{r_{b_o}}^{r_{t_o}} r^2dr - \dot{z}^2\int_{r_{b_o}}^{r_{t_o}} dr), \end{aligned}$$

where ρ is the atmospheric density, C_{Li} is the lift coefficient of the inboard wing C_{Di} is the drag coefficient of the inboard wing, $\bar{c}_i$ is the chord of the inboard wing, r_{b_i} is the distance from the axis of rotation of the stand to the root of the inboard wing, and r_{t_i} is the radial distance from the axis of rotation of the stand to the tip of the inboard wing. Similar definitions apply for the outboard wing.

Using the following relations for the moments about the axis of rotation of the stand,

$$\begin{aligned} \tau_z^s &= -\frac{1}{2}\bar{c}_i\rho\dot{\psi}^2\int_{r_{t_i}}^{r_{b_i}}(C_{Di}c\gamma + C_{Li}s\gamma)r^3dr \\ &\quad -\frac{1}{2}\bar{c}_o\rho\dot{\psi}^2\int_{r_{b_o}}^{r_{t_o}}(C_{Do}c\gamma + C_{Lo}s\gamma)r^3dr \end{aligned}$$

the resultant point of application of the aerodynamic force can be found by

$$r_a = \tau_z^s/(f_x^w c_\gamma + f_z^w s_\gamma). \tag{4}$$

Equation (4) is not constant throughout the flight envelope. However, if the wings are of moderate length, we can the justify the approximation that γ is constant across the wing section. With the additional assumption that the elevator, boom, and ducted fan have a negligible contribution to the wind forces, we end up with only three degrees of freedom: γ, the length of the inboard wing, and the length of the outboard wing. We choose $\gamma = 0$ as the operating condition as well as the inboard wing to be 0.76 m in length. Substituting into equation (4), the solution for the outboard wing length is 0.48 m in order that $r_a = r_s$.

4 Initial Flight Tests

In this section we present some preliminary open loop flight test results of the ducted fan. The purpose of open-loop testing was to get initial starting point for identifying the trim manifold as well as the the longitudinal dynamics of the system.

In order to fly open-loop, the wings were positioned so that the ducted fan is statically stable. The effective gravity of the system was chosen to be 0.075g for the test cases. The user interfaces were set so that the operator could control the commanded current I_m to the motor as well as the thrust vectoring paddles δ_p with the joysticks. The elevator δ_e could be manually controlled by the dSPACE COCKPIT interface.

The two example test cases that will be presented were part of series of tests to determine the trim manifold of the ducted fan for a statically stable configuration. Elevator pulses were given at trimmed conditions in order that we may be able to visualize the short period and phugoid dynamics.

In the first test case, a constant thrust setting of 6.3 ams was chosen. The ducted fan trimmed using the elevator at 5.6 deg and no thrust vectoring paddles at a velocity of approximately 5.4 m/s and angle of attack of 18.3 deg. The ducted fan appeared very stable at this trim condition considering the large disturbances due to the ducted fan flying in its own wake, near the lab wall, and close to the ground. Pulses in the elevator angle between 1 and 20 degrees were used to change the equilibrium position. The ducted fan behaved as expected for small elevator pulses - the system came to equilibrium at a higher altitude. However, in Figure 4 shows a typical result when a pulses larger than 8 degrees are applied to the ducted fan - the ducted fan came to equilibrium at a lower altitude. The large pitch up at nearly constant velocity is characteristic of the short period dynamics. However, for this large elevator pulse, the rapid pitch change resulted in the angle of attack exceeding the stall limit of the wing. Thus, the ducted fan lost lift and the subsequently lost altitude. Although we could identity the short period though the time response in this test case we could not see the typical characteristics of the phugoid - a long period lightly damped oscillation.

In the second test case, we chose a thrust setting of 6.5 amps and trimmed the ducted fan using the thrust vectoring only. The system trimmed at a velocity of approximately 6.5 m/s and thrust vectoring paddles

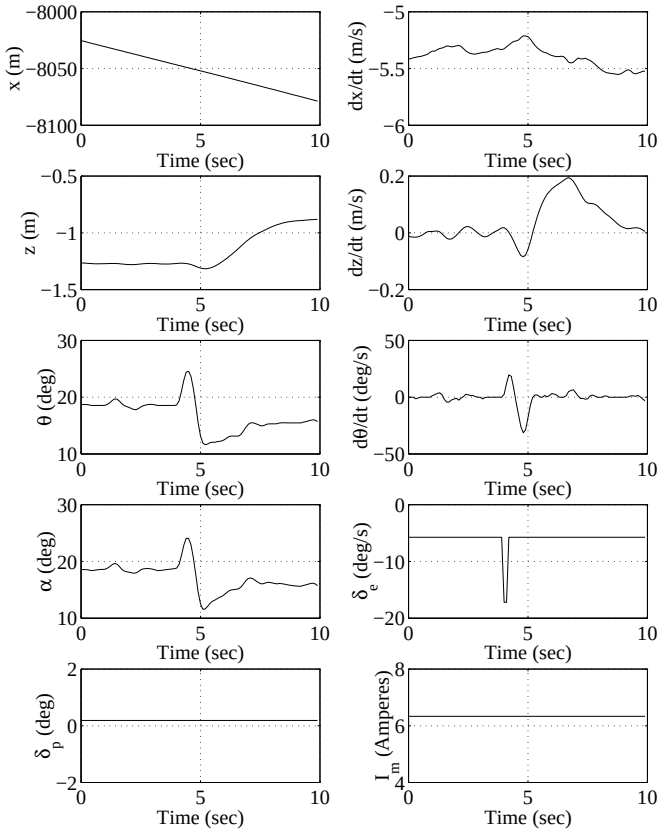

Figure 4: Trim with elevator, response to elevator pulse

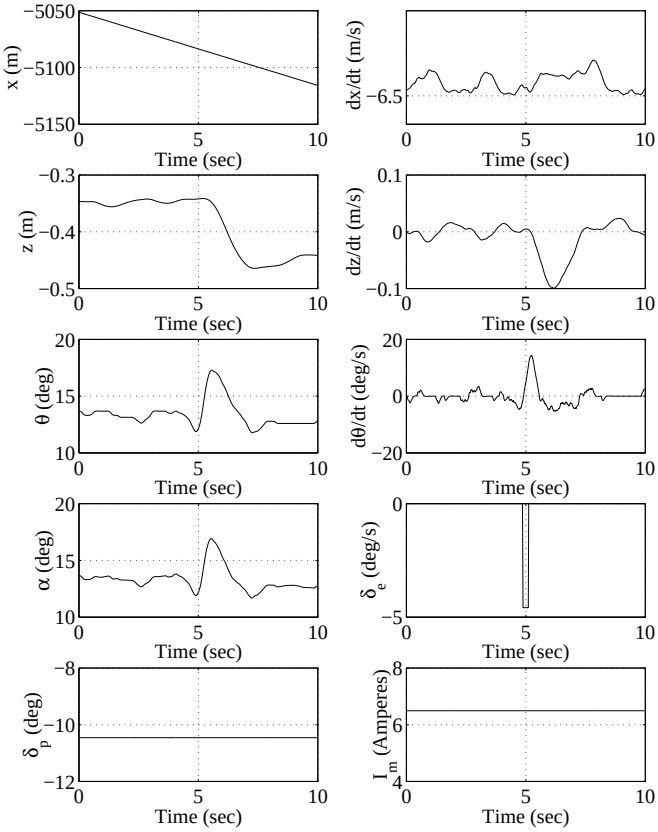

Figure 5: Trim with paddles, response to elevator pulse

at 11 degrees with an angle of attack of 13.5 degrees. Figure 5 shows the response to a 4.7 deg elevator pulse. As in the first test case presented, the short period can be identified but not the phugoid.

Since there was no indication of the phugoid from the time domain analysis, we applied a 4 deg amplitude, 0 to 2 Hz chirp signal to the elevator over a time of 30 sec. This input was chosen in order to identify the natural modes of the system using frequency response techniques. The frequency response plots of the input δ_e to the output $\dot{\theta}$ consistently displayed a mode at .3 rad/sec which likely corresponds to the short period. No other modes could be conclusively identified. It is possible that the phugoid is highly damped at a very low frequency for the ducted fan. If we use Lancester's approximation to the phugoid [6]

$$\omega_n = \sqrt{2}\frac{m_2 g}{m_1 V_0}$$

where V_0 is the trim velocity, we get that $w_n = 0.004$ rad/sec. This low frequency may be very difficult to see given the sensor quantization in θ and the friction in the system.

The results from this preliminary series of flight tests show us that we may want to use a lower effective gravity in order that the system can trim at lower angles of attack. In addition, using a combination of thrust vectoring paddles and elevator may allow us to trim at lower angles of attack. Finally, qualitatively the ducted fan behaves like the longitudinal axis of a flight vehicle. However, much more identification, particularly in determining the stability derivatives, has to be done before any firm conclusions can be drawn concerning the quantitative behavior of the longitudinal modes.

5 Conclusions and Future Work

In this paper we have presented the design and initial flight testing of the Caltech ducted fan. Making the effective mass in the vertical and horizontal directions identical is the crucial design constraint that makes the ducted fan behave like a flight vehicle. Preliminary flight testing indicates that the ducted fan qualitatively exhibits the natural longitudinal dynamics of a flight vehicle.

Work is currently in progress to identify the aerodynamic characteristics of the system. Once the model of ducted fan is completely identified, we will assess the performance of several new flight control theories that

are being developed at Caltech.

6 Acknowledgments

We would like to thank Samuel Chang for his help with the ProE CAD drawings as well as John Hauser for his insightful comments.

References

[1] *dSPACE User Guides*. dSPACE GmbH, Technologiepark 25, D-33100 Paderborn, Germany, document version 3.2 for software version 3.1 edition.

[2] *Popular Mechanics*, First Look at Next-Generation Stealth Fighters, Sep. 1997. Technical Note.

[3] I. Abbott and A. Von Doenhoff. *Theory of Wing Sections*. Dover Publications, 1959.

[4] J.H. Blakelock. *Automatic Control of Aircraft and Missiles*. John Wiley and Sons, Inc, 1965.

[5] H. Choi, P. Sturdza, and R.M. Murray. Design and construction of a small ducted fan engine for nonlinear control experiments. In *Proc. American Control Conference*, pages 2618–2622, 1994.

[6] B. Ektin and L. D. Reid. *Dynamics of Flight*. John Wiley and Sons, Inc, 1996.

[7] C. Lemon and J. Hauser. Design and initial flight test of the Champagne Flyer. In *Proc. American Control Conference*, pages 3852–3859, 1994.

[8] R. Murray, Z. Li, and S. Sastry. *A Mathematical Introduction to Robotic Manipulation*. CRC Press, 1993.

[9] B. Sweetman. Fighters without pilots. *Popular Science*, pages 97–101, Nov. 1997.